

Article

# Rational Control of Spin-Crossover Particle Sizes: From Nano- to Micro-Rods of $[\text{Fe}(\text{Htrz})_2(\text{trz})](\text{BF}_4)$

Lucie Moulet, Nathalie Daro \*, Céline Etrillard, Jean-François Létard, Arnaud Grosjean and Philippe Guionneau \*

CNRS, Univ. Bordeaux, ICMCB, UPR9048, 87, Avenue du Docteur Schweitzer, F-33600 Pessac, France; mouletlucie@gmail.com (L.M.); c.etrillard@gmail.com (C.E.); letard@olikrom.com (J.-F.L.); a.grosjean@uq.edu.au (A.G.)

\* Correspondence: nathalie.daro@icmcb.cnrs.fr (N.D.); philippe.guionneau@icmcb.cnrs.fr (P.G.); Tel.: +33-54-000-2579 (P.G.)

Academic Editor: Guillem Aromí

Received: 13 January 2016; Accepted: 4 February 2016; Published: 24 February 2016

**Abstract:** The spin-crossover (SCO) materials based on iron (II) and triazole ligands can change their spin state under an external perturbation such as temperature, pressure or light irradiation, exhibiting notably large hysteresis in their physical properties' transitions. If these aspects are investigated for decades, it is only in the recent years that the design of SCO particles has attracted the attention of the scientific community with increasing interest focusing on the possibility of getting wide ranges of sizes and shapes of nanoparticles. In this context, we rationalized the reverse-micellar synthesis, thanks to the scrutiny of the experimental parameters, to produce SCO particles with controlled size and shape. This approach has been performed for the reference one-dimensional (1D) polymeric spin-crossover compound of formula  $[\text{Fe}(\text{Htrz})_2(\text{trz})](\text{BF}_4)$ . A synergetic effect of both time and temperature is revealed as being of paramount importance to control the final particle size. Consequently, under well-defined experimental conditions, we can now offer rod-shaped SCO particles with lengths ranging from 75 to 1000 nm.

**Keywords:** spin crossover (SCO); Fe(II) coordination chemistry; nanostructured SCO materials; reverse micelle; 1H-1,2,4-triazole; nanoparticles; rod-like particles; time; temperature

## 1. Introduction

Among all the molecular materials, spin-crossover (SCO) complexes of Fe(II) ions represent an important class of bistable materials for which switching between the high-spin (HS) and the low-spin (LS) electronic configurations can be obtained by diverse external stimuli such temperature, pressure, light irradiation or magnetic field. The switching of the molecular spin-states is accompanied by a spectacular change of various physical properties [1–3]. Of particular interest are the one-dimensional (1D) polymeric  $\text{Fe}^{2+}$  systems  $[\text{Fe}(\text{R-trz})_3]_n \cdot \text{X}_2$  (where R-trz = triazole stands for 4-R-substituted-1,2,4-triazole) since they undergo cooperative thermally-induced LS to HS transitions near room temperature [4–8]. These transitions are accompanied by thermochromism, usually with the LS state being violet/pink and the HS white. These properties allow the consideration of the SCO materials relevant for use in display or switching devices as well as in smart pigments, for instance [9,10]. Furthermore, since these materials are also potential candidates for information storage, electronic devices, pressure or multimodal sensors [11,12], increasing attention has been paid to the elaboration of nanomaterials [13,14] including patterned [15] or continuous [16] thin films, nano-composites [17,18] or nanoparticles. The most convenient synthesis approach to get SCO particles is then based on the reverse-micelle method: microemulsions are used to confine the

growth of the coordination network leading to small particles. Within the literature, a large SCO particle-size spectrum is encountered, running from the nanometer to the millimeter depending on the investigated sample. However, for fundamental studies as well as for practical applications, it still remains an experimental challenge to obtain precise control over the size and the shape of these switchable nanomaterials. Since the first descriptions in 2007 [19–21], a lot of works have been devoted to the influence of experimental synthesis parameters on the morphologies, sizes and properties of the  $[\text{Fe}(\text{R-trz})_3] \cdot \text{X}_2$  SCO materials: for example, parameters such as the surfactant nature [22,23], the surfactant ratio [23–25] and the Fe(II) concentration [26] have been considered. Despite these parameters appearing to influence the final size of the particles, no true rationalization of the synthesis has been done so far. The examination of the reverse-micelle method experimental protocol allowed us to extract two potentially predominant parameters that may impact the size of the final particles. The influence of these parameters, which are the time and the temperature of the reaction, is examined for the compound  $[\text{Fe}(\text{Htrz})_2(\text{trz})](\text{BF}_4)$  ( $\text{Htrz} = 1H\text{-}1,2,4\text{-triazole}$  and  $\text{trz} = \text{deprotonated triazolato ligand}$ ). This well-known compound has been chosen for its chemical stability, its large hysteresis loop between 345 K and 385 K, together with clear evidence that it is possible to get diverse particle sizes from the nano- to the micro-range [13,14,17,18,21,27,28]. In this contribution, we therefore study the influence of these two major experimental parameters on the morphological aspects of the  $[\text{Fe}(\text{Htrz})_2(\text{trz})](\text{BF}_4)$  particles and on their SCO properties.

## 2. Results and Discussion

### 2.1. Experimental Choices and Protocol

In current chemistry, the micelle method is classically used to get nanoparticles as largely described within the literature [29–33]. In this general context, the route for the synthesis of  $[\text{Fe}(\text{R-trz})_3] \cdot \text{X}_2$  SCO nanoparticles is illustrated in Figure 1. Even if this procedure appears quite basic at first sight, many experimental parameters are actually involved such as, for example, the concentrations of the reactant, the surfactant nature and its rate, the mixing protocol, the time and the temperature of the reaction. Regarding these experimental parameters, the reaction time and temperature seem to be the ones with the most influence. Preliminary studies were done to fix other parameters to efficient values [34]. The criteria used to choose and fix the value were the homogeneity of shapes and sizes of the prepared particles. The synthesis can be decomposed into three main steps: (1) preparation of the micellar solutions, (2) reaction/formation of the coordination compound, (3) separation and extraction of the final particles. In our case, the two micellar solutions are first prepared by five minutes of mixing the reactant (iron(II) salt on one part and 1H-1,2,4-triazole on the other part) in water and the chosen surfactant which is Tergitol NP9. For this step, since the present goal is to investigate the time and temperature parameters, the concentrations of the reactant and surfactant ratio have been fixed on the basis of previous studies [34]. The concentrations used are therefore  $1.25 \text{ mol} \cdot \text{L}^{-1}$  for Fe(II) and  $3.75 \text{ mol} \cdot \text{L}^{-1}$  for the ligand while the surfactant rate is fixed at 75%. The two solutions are prepared at the reaction temperature labeled  $T_R$ . Both micellar solutions are then quickly combined and the mixture is stirred during the reaction time labeled  $t_R$ . At the end of that time, the warming is stopped and diethylether is added to block the reaction. The precipitated nanoparticles are recovered by centrifugation, and washed three times with diethylether.

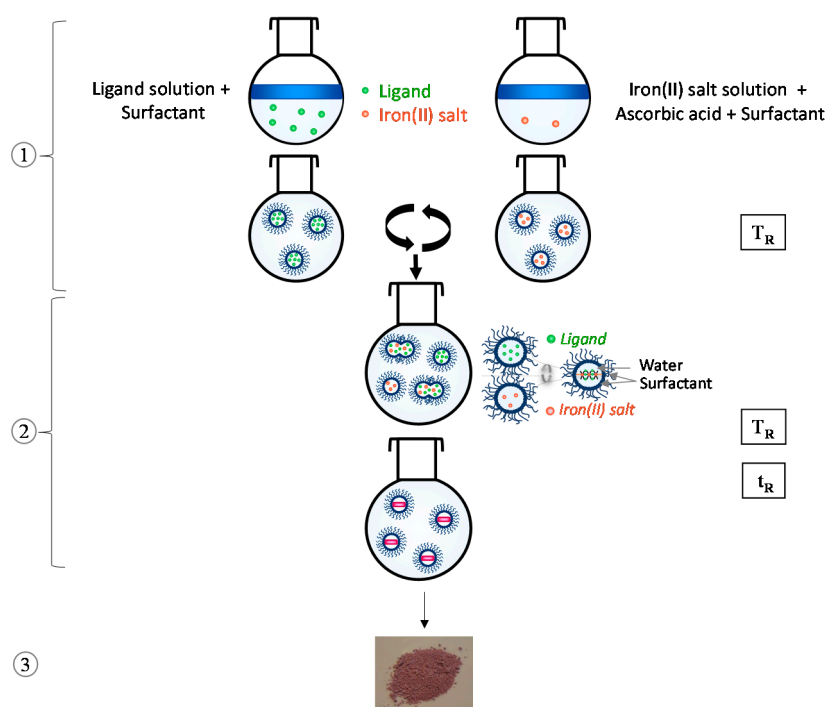


**Figure 1.** Scheme of the experimental process for the synthesis of spin-crossover nanoparticles, here used to get rod-shaped  $[\text{Fe}(\text{Htrz})_2(\text{trz})](\text{BF}_4)$  particles with controlled sizes, playing on the time and temperature of reaction, labeled  $t_R$  and  $T_R$ , respectively. See text for definition of steps (1), (2) and (3).

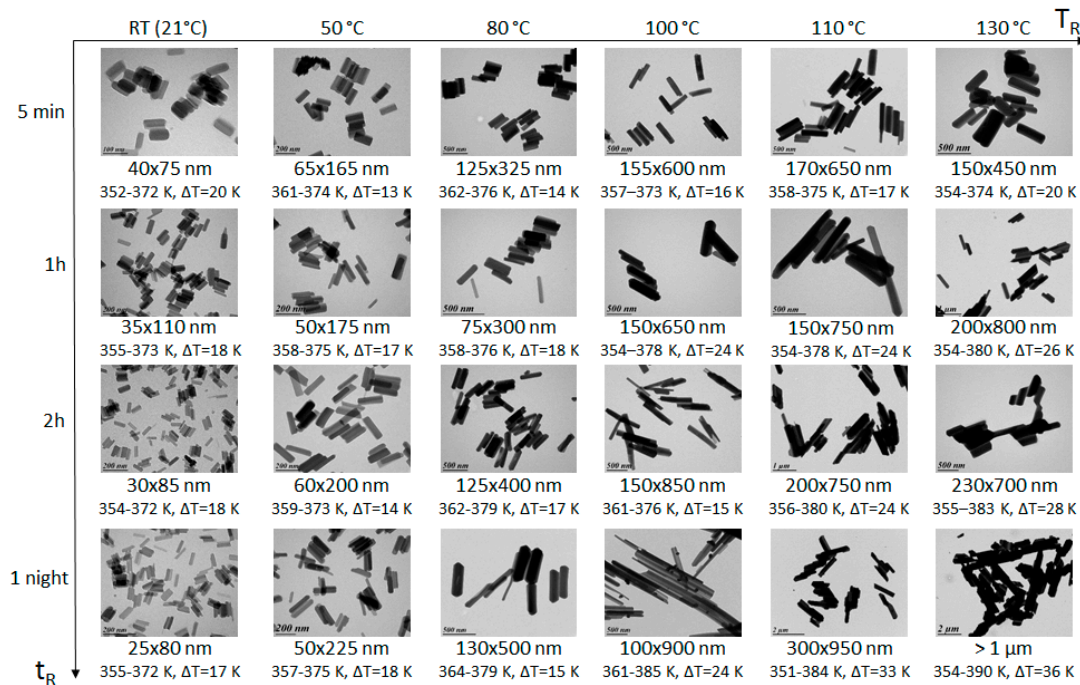


**Figure 2.** Characteristics and properties of the particles of  $[\text{Fe}(\text{Htrz})_2(\text{trz})](\text{BF}_4)$  synthesized with different times and temperatures of reaction ( $t_R$ ,  $T_R$ ): TEM images and deduced particle sizes (width  $\times$  length), SCO features (temperatures and hysteresis width) obtained from magnetic measurements.

A series of synthesis have been implemented by playing on  $t_R$  and  $T_R$ , with only one of these two parameters being modified for each synthesis. Finally, a full ( $t_R$ ,  $T_R$ ) dependence study (Figure 2)

was performed with the  $t_R$  values of five minutes, one hour, two hours and one night combined with the  $T_R$  values of room temperature around 21 °C, 50 °C, 80 °C, 100 °C, 110 °C and 130 °C. The morphologies and sizes of the as-synthesized samples were systematically investigated by TEM. The SCO temperatures of all batches were determined by magnetic measurements in the range of 300–395 K. Figure 2 also displays the characteristics of the batch: TEM images are completed with particle sizes (width  $\times$  length) and SCO temperatures,  $T_{1/2\text{down}}$  and  $T_{1/2\text{up}}$ , corresponding respectively to the cooling and the warming modes, defining the hysteresis loop  $\Delta T$ . In addition, Figure 3 gathers a selection of the magnetic properties representative of the increasing time and temperature effects. Furthermore, the powder X-ray diffraction patterns of each batch are presented in Supplementary Information files (Figures S1 and S2). A selection of the most representative patterns is displayed in Figure 4.

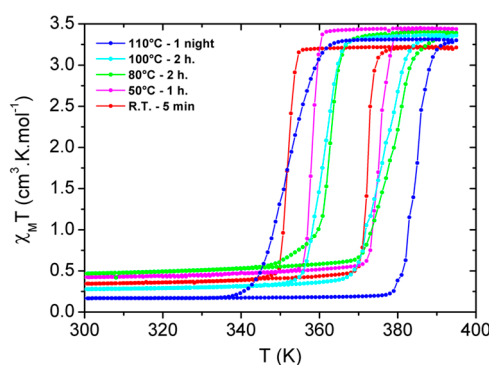


**Figure 3.**  $\chi_M T$  vs.  $T$  plot for some selected batches of  $[\text{Fe}(\text{Htrz})_2(\text{trz})](\text{BF}_4)$  rod-shaped particles obtained at different times and temperatures of reaction  $t_R/T_R$ : 5 min/RT (red), 1 h/50 °C (magenta), 2 h/80 °C (green), 2 h/100 °C (light blue) and one night/110 °C (dark blue).

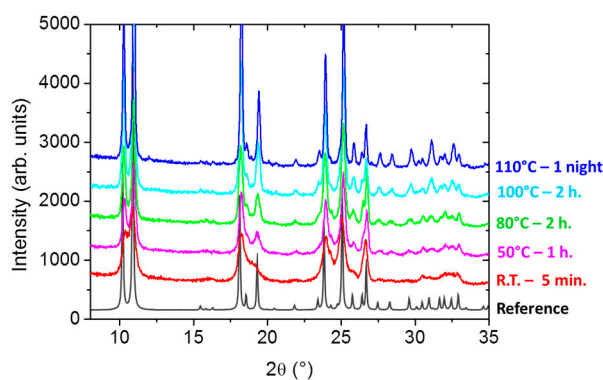


**Figure 4.** X-ray diffraction patterns for some selected batches of  $[\text{Fe}(\text{Htrz})_2(\text{trz})](\text{BF}_4)$  particles obtained at different times and temperatures of reaction ( $t_R, T_R$ ): 5 min/RT (red), 1 h/50 °C (magenta), 2 h/80 °C (green), 2 h/100 °C (light blue), one night/110 °C (dark blue). The diffraction pattern calculated from the crystal structure is also represented as a reference (black).

## 2.2. Morphologies and Sizes of the $[\text{Fe}(\text{Htrz})_2(\text{trz})](\text{BF}_4)$ Particles

From the overview of all the syntheses, all the particles present a similar morphology of rod-like form. Consequently, in our case, the investigated experimental parameters do not influence the external form of the particles. Note that in the literature, the particles of  $[\text{Fe}(\text{Htrz})_2(\text{trz})](\text{BF}_4)$  are always obtained as rods or as spheres; in the latter case, however, it concerns smaller sizes than the ones treated in this work and the true morphology is controversial [35,36]. TEM images allow us to get the sizes of the rods, given here as a width and a length. In the tested ( $t_R, T_R$ ) coupled parameters,

the obtained width lies in the range of 25–300 nm and the length goes from 75 nm to more than 1  $\mu\text{m}$ . If we first consider the reactions performed at the fixed  $T_R$  of the room temperature (21  $^{\circ}\text{C}$ ), when the reaction time  $t_R$  increases, the length of particles is slightly increasing, *i.e.* from 75 nm for a  $t_R$  of 5 min to 80 nm for a  $t_R$  of one night ( $\approx 12$  h), whereas the width is slightly decreasing, *i.e.* from 40 nm to 25 nm, respectively. Consequently, for this value of  $T_R$ , the fluctuations of the sizes appear small. Moreover, the fact that the length does not increase regularly between these two values could show that the increase is therefore not significant. On the contrary, for the batches prepared at 50, 80 and 100  $^{\circ}\text{C}$ , the evolution of the particle sizes as a function of time appears more pronounced and regular. For each temperature series, the particle length is increasing significantly with the time; meanwhile, the width remains quite stable. For example, for the reactions performed at 50  $^{\circ}\text{C}$ , the rod length is increasing regularly from 165 to 225 nm with  $t_R$ , while the rod width remains around 60 nm. These growths can be approximately quantified since the length and the width can be increased by a factor between 4% and 35% at a fixed temperature depending on the chosen ( $t_R$ ,  $T_R$ ) coupling. Furthermore, at the highest temperatures of 110  $^{\circ}\text{C}$  and 130  $^{\circ}\text{C}$ , the longer the  $t_R$ , the bigger the particles. In these cases, length and width are increasing in the same way. This evolution represents 30%–40% for the reactions done at 110  $^{\circ}\text{C}$ . In summary, with the exception of the room temperature, increasing the reaction time allows us to strongly increase the length of the rods and slightly increase their width, with the effects being amplified at high temperature.

Elsewhere, regarding the temperature effect at a fixed reaction time, the particles obtained after a  $t_R$  of five minutes reveal a regular and significant increase of the particle sizes when the media is heated: the width is growing from 40 nm to 150 nm and the length is increasing from 75 nm to 450 nm. This trend can be observed for all the tested values of  $t_R$ . For a given reaction time, the temperature is therefore clearly impacting the particle sizes: the enlargement is around 80% for both dimensions of the particles in the investigated temperature range.

Consequently, it comes out that the choice of the time and temperature of the reaction,  $t_R$  and  $T_R$ , leads to a control of the final sizes of the  $[\text{Fe}(\text{Htrz})_2(\text{trz})](\text{BF}_4)$  rod-shaped particles. More interestingly, all these experiments indicate that time and temperature have a synergetic effect on the particle sizes since the time effects are more pronounced at high temperatures. In other words, the particle sizes increase with the temperature  $T_R$  by an order of magnitude that depends on the fixed value of the time  $t_R$ ; when  $T_R$  increases from 21  $^{\circ}\text{C}$  to 130  $^{\circ}\text{C}$ , the particle length is multiplied by six for a reaction time  $t_R$  of 5 min while it is multiplied by eight for a reaction time  $t_R$  of 2 h. Conversely, at a fixed temperature, the particles grow with the time  $t_R$  by an order of magnitude that increases with the temperature; when  $t_R$  increases from 5 min to one night, the particle length is multiplied by about 1.3 at 50  $^{\circ}\text{C}$  while it is multiplied by 1.5 at 100  $^{\circ}\text{C}$ . In the investigated range, the higher the  $T_R$  and  $t_R$ , the lengthier the particles are.

To conclude, the length of the nanoparticles in the range 75 nm > 1  $\mu\text{m}$  can be precisely tuned by controlling the time and temperature parameters.

### 2.3. Magnetic Properties vs. Size of the Particles

From the SCO properties' point of view, the different particle batches exhibit a sharp transition with the presence of a hysteresis loop as expected for this compound (Figures 2 and 3) [13,14,17,18,21,22,25,27,28,35,36]. Within the investigated ( $t_R$ ,  $T_R$ ) values, the SCO temperatures lay indeed within the known values for this compound with  $T_{1/2\text{up}}$  in the range of 372–390 K and  $T_{1/2\text{down}}$  in the range of 351–364 K. However, some small fluctuations of the SCO temperatures can be noted along with the ( $t_R$ ,  $T_R$ ) variations (Figure 2). At a fixed  $T_R$ , the SCO temperatures do not significantly change with time if  $T_R < 100$   $^{\circ}\text{C}$ , while  $T_{1/2\text{up}}$  increases with time for  $T_R > 100$   $^{\circ}\text{C}$ . In other words,  $T_{1/2\text{up}}$  increases with the volume of the particles, while  $T_{1/2\text{down}}$  is barely affected. As a result, the hysteresis width slightly increases with the particle dimensions, from the narrowest 13 K to the largest 36 K in the present work. This must only be seen as a tendency.

Note that this result is coherent with a recent study of the particle size *vs.* hysteresis width on rod particles of this compound [35] while it slightly differs from recent studies performed on particles that show larger hysteresis [28,36]. However, in the latter case, the investigated particles adopt a different morphology and lay in a smaller size range (< 16 nm). The hysteresis observed here is also slightly narrower than that recently reported for comparable particle dimensions (40 K) [18]. It is, however, worth noting that examination of the whole literature shows that, when comparing SCO temperatures from various studies for this compound, one has to be very careful not to overestimate the significance of small differences, and only tendency must be taken into account. It has been effectively demonstrated that small differences of a few degrees in  $T_{1/2}$  may originate from many experimental parameters, including, for instance, aging of the powder or thermal history of the batch [28,35]. The aim of the present work is not to enter into a detailed description of the origins of the small discrepancy in the SCO temperatures observed in the literature for this compound but to focus on the control of the particle sizes due to the relevant choice of synthesis parameters, which is the ( $t_R$ ,  $T_R$ ) couple. Within this context, the reported SCO temperatures here are within the expected range and show the modification with the particle dimension in relation to the investigated size domain.

#### 2.4. Powder X-ray Diffraction

When dealing with SCO  $[\text{Fe}(\text{R-trz})_3] \cdot X_2$  compounds, it is mandatory to check the crystalline phase since polymorphism is found to be a common trend within this family. To this extend the compound chosen here,  $[\text{Fe}(\text{Htrz})_2(\text{trz})](\text{BF}_4)$ , is an exception since only one crystalline phase has been formally identified so far [37]. In the present case, the diffraction patterns (Figure 4) unambiguously show that whatever the particle size, *i.e.* the chosen experimental synthesis parameters, the crystalline phase is the same and corresponds to the reported one. Bragg peaks appear large, in accordance with the particle sizes, showing an average crystalline quality that is, in any case, lower than the one obtained for the powders optimized for the crystallographic studies performed for  $[\text{Fe}(\text{Htrz})_2(\text{trz})](\text{BF}_4)$  [28,37,38]. Regarding that, it is clear that increasing  $T_R$  slightly improves the crystallinity of the particles.

### 3. Experimental Details

#### 3.1. Synthesis

All reagents and solvents were obtained from commercial sources and used without any further purification. See the core text for the synthesis methodology and choices. All the syntheses have been done with the same procedure, and only the  $T_R$  and  $t_R$  parameters have been changed. Two micellar solutions are first separately prepared. On one hand, 6.3 g of Tergitol NP9 (Sigma, St Louis, MO, USA) are added to a 1.6 mL aqueous solution containing  $\text{Fe}(\text{BF}_4)_2 \cdot 6\text{H}_2\text{O}$  (2 mmol) with a small amount of ascorbic acid (10 mg) at  $T_R$  °C. On the other hand, 6.3 g of Tergitol NP9 (Sigma, St Louis, MO, USA) are added to a 1.6 mL aqueous solution containing 1H-1,2,4-triazole at  $T_R$  °C. The two solutions are mixed and magnetic stirred at  $T_R$  °C during  $t_R$  (min, hours). After the fixed duration, the reaction is stopped by adding diethylether, leading to the particles sedimentation. The violet precipitate is obtained after a first separation with centrifugation at 15,777 rcf during 4 min and three other washings with diethyl ether and centrifugation in the same conditions. The powder is dried at room temperature under ambient atmosphere during one night. Note that from  $T_R > 50$  °C, the reactions are performed under nitrogen atmosphere with a reflux setup and the reaction is stopped by putting the flask in a cold water bath before adding diethylether.

#### 3.2. TEM

Transmission electron microscopy images are acquired using a HITACHI H7650 (Hitachinaka, Japan), with a high resolution mode and a tension of 60 kV. Each batch was analyzed separately and, in order to give the average dimensions of the particles, not less than 100 particles per batch were measured. A meaningful and precise standard deviation on the size is hard to give, though

the mathematical one is often reported. The latter has not much physical sense since it does not take into account experimental parameters, which are surely predominant. The order of magnitude of the standard deviation on the size from the present method is of a few nm [18,36]. This accuracy of knowledge appears by far enough for the discussion developed in the present work. It is clear, however, that a deep analysis of the standard deviations on sizes deduced from TEM measurements is a challenge but should be done, especially when discussing in detail very small particles (< 10 nm).

### 3.3. Magnetic measurements

Variable temperature magnetic data for the powder samples were collected using a Quantum Design MPMS-7S magnetometer (San Diego, CA, USA) under a field of 5000 Oe. Measurements were performed every K in settle mode. The thermal cycles were achieved with a rate of 10 K·min<sup>-1</sup>. The magnetic susceptibility data were used as recorded without diamagnetic contributions. A measurement procedure has been implemented to overcome stabilization problems of the cycle in case of multi-cycle measurement [27]. Indeed, the displacement toward lower temperatures in the heating cycle is a typical behavior, as has already been mentioned for the bulk material [27] as well as for the nanoparticles [21,25]. So, the procedure consists of first warming the compound to 380 K inside the magnetometer, then in maintaining this temperature during 30 minutes and finally starting the measurement given that only one cycle is described between 380 and 300 K.

### 3.4. PXRD

Powder X-ray diffraction measurements have been performed using a PANalytical X'Pert PRO diffractometer (CuK $\alpha$ , X'Celerator detector) (Almelo, The Netherlands) within the range 8° to 80° (2 $\theta$ ) using 60 s exposure with 0.017° steps.

## 4. Conclusions

The target of the present work was to obtain, in a rational manner, a large spectrum of particle sizes by playing on some experimental parameters in the synthesis of the well-known SCO coordination polymer [Fe(Htrz)<sub>2</sub>(trz)](BF<sub>4</sub>). We have chosen to examine the effects of the time and temperature of reaction, labeled  $t_R$  and  $T_R$ , though all other synthesis parameters were fixed. Note that the roles of some of the latter, such as the surfactant ratio, for example, were studied previously [34,35] and that a modification of these parameters may influence the result presented here. A picture of the ( $t_R$ ,  $T_R$ ) effects *vs.* the rod-shaped particle sizes is therefore obtained. The results seem to indicate a synergetic action of these parameters on the growth of the particles since their length increases with the time and temperature of the reaction. The corresponding SCO features are only marginally affected and, finally, it is possible to offer a large panel of sizes for the particles of [Fe(Htrz)<sub>2</sub>(trz)](BF<sub>4</sub>), going from 30 to 1000 nm for the width and from 75 to > 1000 nm for the length, in a control mode.

To conclude, we would like to make some comments. Firstly, it has been recently clearly demonstrated that cycling this compound allows the reduction of the length of the particle [28]. This illustrates how it is ultimately possible to chisel the particles by combining methods. For example, an elegant design of the [Fe(Htrz)<sub>2</sub>(trz)](BF<sub>4</sub>) particles may come from the combination of adequate choices of the synthesis ( $t_R$ ,  $T_R$ ) parameters together with cycling effects. Secondly, the present discussion appears orientated to the increase of the particle size. One of the reasons for this is that, initially, the scope was to get large enough crystallites, if not single crystals, of this compound, and therefore we were tempted to change the direction of the ( $t_R$ ,  $T_R$ ) values to increase the size. Obviously, one can make the reverse arguments and adjust ( $t_R$ ,  $T_R$ ) to decrease the sizes. Elsewhere, the result presented here appears reasonably reproducible since some of the syntheses were performed many times, leading to the same results, *i.e.* the same ( $t_R$ ,  $T_R$ ) values giving the same particle sizes. On the contrary, we tried the same approach to control the particle sizes of [Fe(NH<sub>2</sub>trz)<sub>3</sub>](BF<sub>4</sub>)<sub>2</sub> which is another compound of the SCO coordination polymer Fe-triazole-based family. Attempts were unsuccessful since, in this case, the control of the size using the ( $t_R$ ,  $T_R$ ) parameters is highly perturbed

by the polymorphism shown in this compound. These remarks highlight once more the outstanding position of  $[\text{Fe}(\text{Htrz})_2(\text{trz})](\text{BF}_4)$  within the SCO materials.

**Acknowledgments:** Acknowledgements are due to the Conseil Régional d'Aquitaine for the PhD grants of A.G. and L.M and to the ANR agency (project ANR-11-BS08-06) for funding. The microscopy was done in the Bordeaux Imaging Center of the University of Bordeaux. The help of Sabrina Lacomme is acknowledged. The X-ray diffraction is performed at the XRD center of ICMCB.

**Author Contributions:** All authors contributed equally to the experimental work. The paper was written by Nathalie Daro and Philippe Guionneau.

**Conflicts of Interest:** The authors declare no conflict of interest.

## References

1. Gütlich, P.; Goodwin, H.A. Spin crossover-An overall perspective. *Top. Curr. Chem.* **2004**, *233*, 1–47.
2. Halcrow, M.A., Ed.; *Spin-Crossover Materials: Properties and Applications*; John Wiley & Sons: Chichester, UK, 2013.
3. Gütlich, P.; Gaspar, A.B.; Garcia, Y. Spin state switching in iron coordination compounds. *Beilstein J. Org. Chem.* **2013**, *9*, 342–391. [[CrossRef](#)] [[PubMed](#)]
4. Aromí, G.; Barrios, L.A.; Roubeau, O.; Gamez, P. Triazoles and tetrazoles: Prime ligands to generate remarkable coordination materials. *Coord. Chem. Rev.* **2011**, *255*, 485–546. [[CrossRef](#)]
5. Roubeau, O. Triazole-based one-dimensional spin-crossover coordination polymers. *Chem. Eur. J.* **2012**, *18*, 15230–15244. [[CrossRef](#)] [[PubMed](#)]
6. Lavrenova, L.G.; Shakirova, O.G. Spin crossover and thermochromism of iron(II) coordination compounds with 1,2,4-triazoles and tris(pyrazol-1-yl)methanes. *Eur. J. Inorg. Chem.* **2013**, *2013*, 670–682. [[CrossRef](#)]
7. Haasnoot, J.G.; Vos, G.; Groeneveld, W.L. 1,2,4-triazole complexes, III Complexes of transition metal(II) nitrates and fluoroborates. *Z. Naturforschung* **1977**, *32b*, 1421–1430. [[CrossRef](#)]
8. Kahn, O.; Kröber, J.; Jay, C. Spin transition molecular materials for displays and data recording. *Adv. Mater.* **1992**, *4*, 718–728. [[CrossRef](#)]
9. Kahn, O.; Jay Martinez, C. Spin-transition polymers: From molecular materials toward memory devices. *Science* **1998**, *279*, 44–48. [[CrossRef](#)]
10. Létard, J.F.; Guionneau, P.; Goux-Capes, L. Towards spin crossover applications. *Top. Curr. Chem.* **2004**, *235*, 221–249.
11. Linares, J.; Coddjovi, E.; Garcia, Y. Pressure and temperature spin crossover sensors with optical detection. *Sensors* **2012**, *12*, 4479–4492. [[CrossRef](#)] [[PubMed](#)]
12. Gentili, D.; Demitri, N.; Schäfer, B.; Liscio, F.; Bergenti, I.; Ruani, G.; Ruben, M.; Cavallini, M. Multi-modal sensing in spin crossover compounds. *J. Mater. Chem. C* **2015**, *3*, 7836–7844. [[CrossRef](#)]
13. Shepherd, H.J.; Molnár, G.; Nicolazzi, W.; Salmon, L.; Bousseksou, A. Spin crossover at the nanometer scale. *Eur. J. Inorg. Chem.* **2013**, *2013*, 653–661. [[CrossRef](#)]
14. Martinho, P.N.; Rajnak, C.; Ruben, M. Nanoparticles, thin films and surface patterns from spin-cross-over materials and electrical spin state control. In *Spin-Crossover Materials: Properties and Applications*, 1st ed.; Halcrow, M.A., Ed.; John Wiley & Sons: Chichester, UK, 2013; pp. 375–404.
15. Quintero, C.M.; Gural'skiy, I.A.; Salmon, L.; Molnár, G.; Bergaud, C.; Bousseksou, A. Soft lithographic patterning of spin crossover complexes. Part 1: Fluorescent detection of the spin transition in single nano-objects. *J. Mater. Chem.* **2012**, *22*, 3745–3751. [[CrossRef](#)]
16. Sereidyuk, M.; Gaspar, A.B.; Ksenofontov, V.; Reiman, S.; Galyametdinov, Y.; Haase, W.; Rentschler, E.; Gütlich, P. Room temperature operational thermochromic liquid crystals. *Chem. Mater.* **2006**, *18*, 2513–2519. [[CrossRef](#)]
17. Faulmann, C.; Chahine, J.; Malfant, I.; Caro, D.; Cormary, B.; Valade, L. A facile route for the preparation of nanoparticles of the spin-crossover complex  $[\text{Fe}(\text{Htrz})_2(\text{trz})](\text{BF}_4)$  in xerogel transparent composite film. *Dalton Trans.* **2011**, *40*, 2480–2485. [[CrossRef](#)] [[PubMed](#)]
18. Herrera, J.M.; Titos-Padilla, S.; Pope, S.J.A.; Berlanga, I.; Zamora, F.; Delgado, J.J.; Kamenev, K.V.; Wang, X.; Prescimone, A.; Brechin, E.K.; *et al.* Studies on bifunctional Fe(II)-triazole spin crossover nanoparticles: Time-dependent luminescence, surface grafting and the effect of silica shell and hydrostatic pressure on the magnetic properties. *J. Mater. Chem. C* **2015**, *3*, 7819–7829. [[CrossRef](#)]

19. Létard, J.F.; Daro, N.; Nguyen, O. Nanoparticles of a spin transition compound. Patent WO2007/065996, 14 June 2007.
20. Forestier, T.; Mornet, S.; Daro, N.; Nishihara, T.; Mouri, S.I.; Tanaka, K.; Fouché, O.; Freysz, E.; Létard, J.F. Nanoparticles of iron(II) spin-crossover. *Chem. Commun.* **2008**, 4327–4329. [[CrossRef](#)] [[PubMed](#)]
21. Coronado, E.; Galán-Mascarós, J.R.; Monrabal-Capilla, M.; García-Martínez, J.; Pardo-Ibañez, P. Bistable spin-crossover nanoparticles showing magnetic thermal hysteresis near room temperature. *Adv. Mater.* **2007**, *19*, 1359–1361. [[CrossRef](#)]
22. Mader, D.; Pillet, S.; Carteret, C.; Stébé, M.J.; Blin, J.L. Confined growth of spin crossover nanoparticles in surfactant-based matrices: Enhancing shape anisotropy. *J. Dispers. Sci. Sci. Technol.* **2011**, *32*, 1771–1779. [[CrossRef](#)]
23. Gural'skiy, I.A.; Quintero, C.M.; Molnár, G.; Fritsky, I.O.; Salmon, L.; Bousseksou, A. Synthesis of spin-crossover nano- and micro-objects in homogeneous media. *Chem. Eur. J.* **2012**, *18*, 9946–9954. [[CrossRef](#)] [[PubMed](#)]
24. Forestier, T.; Kaiba, A.; Pechev, S.; Denux, D.; Guionneau, P.; Etrillard, C.; Daro, N.; Freysz, E.; Létard, J.F. Nanoparticles of  $[\text{Fe}(\text{NH}_2\text{-trz})_3]\text{Br}_2 \cdot 3\text{H}_2\text{O}$  ( $\text{NH}_2\text{-trz}$  = 4-amino-1,2,4-triazole) prepared by the reverse micelle technique: Influence of particle and coherent domain size on spin-crossover properties. *Chem. Eur. J.* **2009**, *15*, 6122–6130. [[CrossRef](#)] [[PubMed](#)]
25. Galán-Mascarós, J.R.; Coronado, E.; Forment-Aliaga, A.; Monrabal-Capilla, M.; Pinilla-Cienfuegos, E.; Ceolin, M. Tuning size and thermal hysteresis in bistable spin crossover nanoparticles. *Inorg. Chem.* **2010**, *49*, 5706–5714. [[CrossRef](#)] [[PubMed](#)]
26. Tokarev, A.; Salmon, L.; Guari, Y.; Molnár, G.; Bousseksou, A. Synthesis of spin crossover nano-objects with different morphologies and properties. *New J. Chem.* **2011**, *35*, 2081–2088. [[CrossRef](#)]
27. Kröber, J.; Audière, J.P.; Claude, R.; Codjovi, E.; Kahn, O.; Haasnoot, J.G.; Grolière, F.; Jay, C.; Bousseksou, A.; Linares, J.; *et al.* Spin transitions and thermal hystereses in the molecular-based materials  $[\text{Fe}(\text{Htrz})_3](\text{BF}_4)_2 \cdot \text{H}_2\text{O}$  ( $\text{Htrz}$  = 1,2,4-*H*-triazole; 1,2,4-triazolato). *Chem. Mater.* **1994**, *6*, 1404–1412. [[CrossRef](#)]
28. Grosjean, A.; Daro, N.; Pechev, S.; Moulet, L.; Etrillard, C.; Chastanet, G.; Guionneau, P. The spin-crossover phenomenon at the coherent-domains scale in 1D polymeric powders: Evidence for a structural fatigability. *Eur. J. Inorg. Chem.* **2016**. [[CrossRef](#)]
29. Pileni, M.P. *Reverse Micelles*; Elsevier: Amsterdam, The Netherlands, 1989.
30. Tanford, C. Micelle shape and size. *J. Phys. Chem.* **1972**, *76*, 3020–3024. [[CrossRef](#)]
31. Ganguli, A.K.; Ganguly, A.; Vaidya, S. Microemulsion-based synthesis of nanocrystalline materials. *Chem. Soc. Rev.* **2010**, *39*, 474–485. [[CrossRef](#)] [[PubMed](#)]
32. Dwars, T.; Paetzold, E.; Oehme, G. Reactions in micellar systems. *Angew. Chem. Int. Ed.* **2005**, *44*, 7174–7199. [[CrossRef](#)] [[PubMed](#)]
33. Paul, B.K.; Moulik, S.P. Uses and applications of microemulsions. *Curr. Sci.* **2001**, *80*, 990–1001.
34. Etrillard, C. Synthèse de Nanoparticules à Transition de Spin et Étude des Propriétés. Application en Électronique Moléculaire. Ph.D. Thesis, University of Bordeaux, Talence, France, 2011.
35. Bartual-Murgui, C.; Natividad, E.; Roubeau, O. Critical assessment of the nature and properties of Fe(II) triazole-based spin-crossover nanoparticles. *J. Mater. Chem. C* **2015**, *3*, 7916–7924. [[CrossRef](#)]
36. Gimenez-Marqués, M.; Garcia-Sanz de Larrea, M.L.; Coronado, E. Unravelling the chemical design of spin-crossover nanoparticles based on iron(II)–triazole coordination polymers: Towards a control of the spin transition. *J. Mater. Chem. C* **2015**, *3*, 7946–7953. [[CrossRef](#)]
37. Grosjean, A.; Négrier, P.; Bordet, P.; Etrillard, C.; Mondieig, D.; Pechev, S.; Lebraud, E.; Létard, J.F.; Guionneau, P. Crystal structures and spin crossover in the polymeric material  $[\text{Fe}(\text{Htrz})_2(\text{trz})](\text{BF}_4)$  including coherent-domain size reduction effects. *Eur. J. Inorg. Chem.* **2013**, 796–802. [[CrossRef](#)]
38. Durand, P.; Pillet, S.; Bendeif, E.E.; Carteret, C.; Bouzaoui, M.; El Hamzaoui, H.; Capoen, B.; Salmon, L.; Hébert, S.; Ghanbaja, J.; *et al.* Room temperature bistability with wide thermal hysteresis in a spin crossover silica nanocomposite. *J. Mater. Chem. C* **2013**, *1*, 1933–1942. [[CrossRef](#)]

